Geochemical Perspectives Letters

K-Ca dating and Ca isotope composition of the oldest Solar System lava, Erg Chech 002

W. Dai, F. Moynier, L. Fang, J. Siebert

Supplementary Information

The Supplementary Information includes:

- Sample and Analytical Methods
- Ca Isotope Fractionation During Partial Melting of the EC 002 Parent Body
- Tables S-1 to S-4
- Figures S-1 to S-5
- Supplementary Information References

Sample and Analytical Methods

Erg Chech 002 andesite meteorite. Erg Chech 002 is unbrecciated with a medium-grained groundmass which suggests a crystallisation within a thick flow or in a shallow intrusion. The shocked stage of EC 002 is M-S2 (Barrat *et al.*, 2021), which points to a post-shock temperature of EC 002 lower than 200 °C without later metamorphism (Stöffler *et al.*, 2018). The whole rock consists of 45 % Na-rich plagioclase with lamellae of K-rich feldspar, 38 % anhedral pyroxene, about 5 % interstitial silica minerals and other accessory minerals. The samples are rather fresh with little rusty appearance on silicate minerals. The pyroxenes in the groundmass are generally augitic with fine exsolutions of low-Ca pyroxene. The total CaO content is 12.0–15.1 % and K_2O content is almost negligible (<0.03 %). The feldspars are totally albitic with lamellae of K-rich feldspar. The typical plagioclases contain about 4.45 % CaO and 0.47 % K_2O while some K-rich grains could also be observed. The exsolutions of these minerals indicates that the whole rock experienced subsolidus re-equilibration during its cooling down which may last for several hundred years (Barrat *et al.*, 2021). The total K/Ca ratio of pyroxenes and plagioclase are distinct which is ideal for K-Ca dating.

The samples were crushed into small grains and different fragments were separated. Two pyroxene fractions and three plagioclase fractions were selected together with two bulk rock fractions for Ca isotope analysis. All of these minerals fractions have been previously used for ^{26}Al-^{26}Mg and ^{147}Sm-^{143}Nd dating (Fang *et al.*, 2022). These fractions could be regarded as mixture of fragments from different mineral grains. The pyroxenes are K-poor with very low K/Ca ratios (K/Ca = 0.0072 and 0.0213). The K/Ca ratios of plagioclases (K/Ca = 0.1836–0.3926) selected are higher than that of typical plagioclases (K/Ca = 0.1227). The absence of correlation between CaO and K_2O content of these fractions suggest that these fractions are not a simple mixture of typical pyroxenes and plagioclases, and the high K/Ca ratios of plagioclase fractions actually represent the K-rich grains that are distinct from typical plagioclases (Figure S-1).

Chemical purification. The detailed description has been documented in previous studies (Dai *et al*., 2022) and we provide a short summary here. All the samples were aliquots containing ~10 mg Ca which have previously been used for ^{147}Sm-^{143}Nd dating (Fang *et al.*, 2022). The solutions were dried down and redissolved in 4 mol/L HNO_3 in preparation for the chemical purification on a column filled up with 250 µL of Eichrom DGA resin. After washing the columns, the samples were loaded in 0.4 mL of 4 mol/L HNO_3, which contain ~5 mg Ca. The matrix elements were washed by further addition of 6.75 mL of 4 mol/L HNO_3, and the Ca fraction was collected with 3 mL of water. This procedure was performed twice. Then the Ca fraction were further purified from Sr by passing through ~100 µL of Eichrom Sr spec resin. After washing the resin, the samples were loaded in 0.5 mL of 3 mol/L HNO_3, and the calcium was then collected with an additional 1.5 mL of 3 mol/L HNO_3. This collected Ca fraction was dried down at 120 °C. Several drops of concentrated HNO_3 were added and evaporated to decompose potential organic matters leached during the column chemistry. The samples were finally redissolved in 0.5 mol/L HNO_3 for analysis on the MC-ICP-MS, Nu Sapphire.

Calcium isotope measurement on the Nu Sapphire. The detailed information for Ca isotope measurement on Nu Sapphire that is followed here has been already documented (Dai *et al.*, 2022). In this study, to get higher precision on radiogenic ^{40}Ca anomaly, all the measurements were conducted on Ca solution with a concentration of 200 ppb, which yield total Ca signal over 300 V. The ^{40}Ca, ^{42}Ca, ^{43}Ca and ^{44}Ca ion beams were measured using Faraday cups at L6, L1, H3 and H6. Meanwhile, the intensities of the mass 41 ($^{41}K^{+}$) and 43.5 ($^{87}Sr^{++}$) were monitored on Faraday cups L5 and H5. Each analysis consisted of a 60-second zero measurement in 0.5 mol/L HNO_3, followed by one block of 30 cycles with 5 second integrations. A 100-second wash was performed in 0.5 mol/L HNO_3 following each standard and sample analysis and a transfer time of 90 seconds was applied. In these conditions, the background on the mass 40 was ~700 mV. The signal on the mass 41 was approximatively 25 mV. Each sample was measured between 5 to 12 times in a sequence. The mass bias was corrected by measuring the samples alternatively with the SRM 915b standard solution (standard-sample bracketing).

We report the mass-dependent deviation and the radiogenic Ca anomaly at the same time. For mass-dependent deviation, the data is presented as $\delta^{x/44}$Ca:

$$\delta^{x/44}\mathrm{Ca} = \left(\frac{(^{x}\mathrm{Ca}/^{44}\mathrm{Ca})_{\mathrm{sample}}}{(^{x}\mathrm{Ca}/^{44}\mathrm{Ca})_{\mathrm{SRM\ 915b}}} - 1\right) \times 10^{3}$$

with x = 40, 42, or 43. While the radiogenic input on ^{40}Ca is reported using the epsilon notation as:

$$\varepsilon^{40}\mathrm{Ca} = \left(\frac{(^{40}\mathrm{Ca}/^{44}\mathrm{Ca})_{\mathrm{n\ sample}}}{(^{40}\mathrm{Ca}/^{44}\mathrm{Ca})_{\mathrm{n\ SRM\ 915b}}} - 1\right) \times 10^{4}$$

with (^{40}Ca/^{44}Ca)n representing the ^{40}Ca/^{44}Ca ratio corrected from the mass-dependent isotopic fractionation after being normalised to the ^{42}Ca/^{44}Ca ratio using the exponential law and a ^{42}Ca/^{44}Ca ratio of 0.31221 (Russell *et al.*, 1978). The effect of concentration mismatch on Sapphire is more significant than on other MC-ICP-MS and such effect could be variable due to the modification of tuning parameter at the beginning of each session. To avoid the concentration mismatch effect, a simple correction was performed based on method from Dai *et al.* (2022) (see Figure S-2).

In this study, all the data have been acquired using SRM 915b as the standard because the original SRM 915a standard is not commercially available anymore. However, most of the Ca isotope data in literatures was reported against SRM 915a. To facilitate comparison, the $\delta^{44/40}$Ca and ε^{40}Ca of EC 002 separates in this study have been renormalised to SRM 915a. The difference in $\delta^{44/40}$Ca and ε^{40}Ca of the SRM 915b compared to SRM 915a are 0.72 ‰ and −0.46 ε-units, respectively (see Table S-2 and references therein). To avoid the radiogenic ^{40}Ca effect on the $\delta^{44/40}$Ca value, the value is calculated based on $\delta^{44/40}\mathrm{Ca}_{\mathrm{SRM\ 915a}} = 0.72 - \delta^{42/44}\mathrm{Ca} \times 2.048$. It should be noted that the ^{40}Ca/^{44}Ca ratio of SRM 915a measured by TIMS from different laboratories also show small variations (e.g., Simon *et al.*, 2009; He *et al.*, 2017; Mills *et al.*, 2018; Antonelli and Simon, 2020; Antonelli *et al.*, 2021). The small deviation may be caused by different analytical methods, correction laws or potential heterogeneity in SRM 915a (Schiller *et al.*, 2012; Naumenko-Dèzes *et al.*, 2015). Therefore, to compare MC-ICP-MS data with Thermo-Ionisation Mass-Spectrometers (TIMS) data, we suggest using an average ^{40}Ca/^{44}Ca ratio (^{40}Ca/^{44}Ca = 47.1622) calculated from literature data and to re-calculate the ^{40}Ca/^{44}Ca (^{40}Ca/^{44}Ca = 47.1600, ε^{40}Ca = −0.46 relative to SRM 915a) of NIST SRM 915b (Schiller *et al.*, 2012; Naumenko-Dèzes *et al.*, 2015; He *et al.*, 2017; Antonelli *et al.*, 2021). All the ε^{40}Ca of Erg Chech 002 separates were then renormalised to this value to get accurate and comparable ^{40}Ca/^{44}Ca ratios.

Two USGS reference materials (BHVO-2, GSP-2) were digested, purified and analysed during the same sequences as the other samples (Table S-1). The GSP-2 is a well-suited sample to access the accuracy and precision of $\varepsilon^{40}Ca$ because it has a large ^{40}Ca excess and was measured together with EC 002 samples in each session from February 2022 to April 2022 (Table S-2). Two standard error of $\varepsilon^{40}Ca$ in most sessions is better than 0.4 ε-unit (n = 60). The $\delta^{44/40}Ca$ and $\varepsilon^{40}Ca$ of the two USGS standards are consistent with literature data within the external analytical uncertainty (Schiller *et al.*, 2012; Valdes *et al.*, 2014; Amsellem *et al.*, 2017; He *et al.*, 2017; Liu *et al.*, 2017; Lanping *et al.*, 2018; Li *et al.*, 2018).

Ca Isotope Fractionation During Partial Melting of the EC 002 Parent Body

Previous studies on calculating the Ca isotope fractionation during partial melting of terrestrial mantle rocks are mainly based on incremental non-modal batch melting model with modal composition of the residue recalculated at each melting increment (Williams and Bizimis, 2014; Chen *et al.*, 2019; Wang *et al.*, 2019).

Here we assume chondritic component as the starting material of partial melting of EC 002. The initial CaO content is set to be 2.05 % and the initial mineral proportion is $Ol_{0.55}$ + $Opx_{0.23}$ + $Cpx_{0.07}$ + $Pl_{0.07}$ + $Metal_{0.08}$. The melting model were roughly determined by experimental result (Collinet and Grove, 2020). It has two steps:

$$0.55\ Cpx + 0.75\ Pl = 0.18\ Ol + 0.12\ Opx + 1\ Melt \text{ (when Pl and Cpx exist in the source)}$$

$$0.5\ Ol + 0.5\ Opx = 1\ Melt \text{ (after the consumption of Pl and Cpx)}$$

The partition coefficient values $K_d^{mineral/melt}$ for different minerals are from GERM database (https://kdd.earthref.org/KdD, and references there in). To better match the experimental results, the $K_d^{mineral/melt}$ were slightly modified within the range determined by different studies. As is shown in Figure S-4, the aggregated melt we obtained in this study match the experimental results (except for that under low melting degree which could be attributed to rapid extraction of alkaline elements at the start of melting).

Here, we assume the $\delta^{44/40}Ca$ of initial material is 0.94 ‰ which is consistent with average value of most non-carbonaceous chondrites (Antonelli and Simon, 2020; Valdes *et al.*, 2021). The Ca isotope fractionation between different minerals is based on theoretical prediction of equilibrium Ca isotope fractionation under a fixed temperature of 1224 °C (Wang *et al.*, 2017; Zhang *et al.*, 2018; Huang *et al.*, 2019). This is estimated by the bulk MgO content of EC 002 and the correlation between MgO and temperature from experiments (Collinet and Grove, 2020; Barrat *et al.*, 2021). Our result suggests that the Ca isotope fractionation between EC 002 and its parent body is smaller than 0.10 ‰ and the aggregated melt at 25 % melting degree is 0.86 ‰, highly consistent with EC 002 (Table S-4, Figure S-4). It further supports that the $\delta^{44/40}Ca$ of EC 002 parent body is 0.94 ± 0.05 ‰, point to a non-carbonaceous chondritic source material.

Supplementary Tables

Table S-1 Ca isotopic compositions and K/Ca ratios of mineral separates from Erg Chech 002.

Sample name	$\delta^{40/44}Ca$[1] (‰)	2 s.d.	$\delta^{42/44}Ca$ (‰)	2 s.d.	$\delta^{43/44}Ca$ (‰)	2 s.d.	*n*	$\delta^{44/40}Ca$ (SRM 915a)[2]	2 s.d.	$\varepsilon^{40}Ca$ (SRM 915b)	$\varepsilon^{40}Ca$ (SRM 915a)[3]	2 s.e.	$^{40}K/^{44}Ca$	2 s.e.	$^{40}Ca/^{44}Ca$[4]	2 s.e.	CaO (wt. %)	K_2O (wt. %)
WR1 (bulk rock)	-0.07	0.13	-0.06	0.10	-0.02	0.14	9			0.61		0.27			47.16289	0.00128		
	-0.09	0.10	-0.10	0.07	-0.05	0.05	8			1.16		0.17			47.16549	0.00079		
	-0.08	0.06	-0.08	0.06	-0.01	0.06	6			0.85		0.68			47.16399	0.00322		
mean	-0.08	0.02	-0.08	0.04	-0.02	0.05		0.88	0.07	0.87	0.41	0.32	0.000330	0.000013	47.16412	0.00151	6.32	0.31
WR2 (bulk rock)	0.02	0.10	-0.07	0.07	-0.02	0.03	9			1.60		0.16			47.16755	0.00076		
	0.01	0.11	-0.03	0.07	0.00	0.05	8			0.73		0.22			47.16346	0.00105		
	-0.11	0.29	-0.08	0.27	0.00	0.17	12			0.50		0.84			47.16237	0.00397		
mean	-0.03	0.15	-0.06	0.05	-0.01	0.03		0.85	0.11	0.95	0.49	0.67	0.000390	0.000011	47.16446	0.00315	7.70	0.44
D>3.3 (pyroxene)	-0.13	0.09	-0.07	0.07	-0.03	0.04	10			0.14		0.23			47.16068	0.00109		
	-0.12	0.09	-0.07	0.09	-0.03	0.10	5			0.27		0.59			47.16125	0.00277		
mean	-0.13	0.01	-0.07	0.00	-0.03	0.00		0.87	0.00	0.20	-0.26	0.12	0.000042	0.000004	47.16096	0.00058	13.2	0.08
Px1 (pyroxene)	-0.04	0.17	-0.04	0.15	0.02	0.09	8			0.32		0.62			47.16153	0.00294		
	-0.10	0.09	-0.08	0.06	-0.03	0.06	7			0.69		0.28			47.16326	0.00131		
	0.03	0.06	-0.02	0.08	-0.02	0.07	7			0.68		0.54			47.16319	0.00255		
mean	-0.04	0.13	-0.05	0.06	-0.01	0.06		0.82	0.12	0.56	0.10	0.24	0.000124	0.000007	47.16266	0.00113	9.85	0.18
Plg1 (plagioclase)	0.31	0.30	0.02	0.26	0.02	0.18	8			2.69		0.76			47.17271	0.00358		
Replicate	0.27	0.05	0.02	0.01	0.02	0.07	5			2.35		0.17			47.17108	0.00082		
mean	0.29	0.05	0.02	0.01	0.02	0.00		0.68	0.01	2.52	2.06	0.35	0.001069	0.000037	47.17189	0.00163	3.92	0.62
Plg3 (plagioclase)	0.13	0.04	-0.07	0.05	-0.03	0.06	9			2.78		0.26			47.17313	0.00120		
	0.19	0.05	-0.05	0.06	-0.05	0.09	5			2.98		0.30			47.17405	0.00142		
mean	0.16	0.08	-0.06	0.02	-0.04	0.03		0.84	0.05	2.88	2.42	0.20	0.001342	0.000048	47.17359	0.00092	3.96	0.79
Plg0 (plagioclase)	0.60	0.13	0.01	0.09	0.01	0.16	6			5.35		0.41			47.18523	0.00193		
	0.56	0.14	0.02	0.10	0.01	0.02	9			5.29		0.28			47.18495	0.00131		
	0.43	0.05	-0.04	0.07	-0.03	0.03	5			5.06		0.63			47.18385	0.00295		
	0.50	0.09	0.00	0.11	-0.01	0.09	6			5.00		0.71			47.18356	0.00336		
mean	0.52	0.15	0.00	0.05	-0.01	0.04		0.72	0.10	5.17	4.71	0.17	0.002286	0.000071	47.18440	0.00081	2.47	0.84

Table S-1 continued.

Sample name	$\delta^{40/44}Ca$[1] (‰)	2 s.d.	$\delta^{42/44}Ca$ (‰)	2 s.d.	$\delta^{43/44}Ca$ (‰)	2 s.d.	*n*	$\delta^{44/40}Ca$ (SRM 915a)[2]	2 s.d.	$\varepsilon^{40}Ca$ (SRM 915b)	$\varepsilon^{40}Ca$ (SRM 915a)[3]	2 s.e.	$^{40}K/^{44}Ca$	2 s.e.	$^{40}Ca/^{44}Ca$[4]	2 s.e.	CaO (wt. %)	K_2O (wt. %)
Geostandards																		
BHVO-2	-0.09	0.12	-0.03	0.08	-0.02	0.06	9	0.78	0.12	-0.26	-0.72	0.20						
GSP-2	0.53	0.12	0.05	0.06	0.01	0.08	60	0.62	0.12	4.22	3.76	0.12						
915b	0.00	0.11	0.00	0.10	0.00	0.09	201	0.72		-0.01	-0.47	0.09						

[1] The Ca isotope ratio are normalised to SRM 915b.
[2] To avoid the radiogenic ^{40}Ca effect, the value is calculated based on $\delta^{44/40}Ca_{SRM\ 915a} = 0.72 - \delta^{42/44}Ca \times 2.048$.
[3] The $\varepsilon^{40}Ca$ of SRM 915a is 0.46 less than that of SRM 915b in the literature.
[4] The $^{40}Ca/^{44}Ca$ values are recalculated based on a fixed $^{40}Ca/^{44}Ca$ value for SRM 915b ($^{40}Ca/^{44}Ca = 47.1600$).

Table S-2 Ca isotope data for GSP-2 measured in different sessions.

Analytical date	$\delta^{40/44}$Ca (SRM 915b)	$\delta^{42/44}$Ca (SRM 915b)	$\delta^{43/44}$Ca (SRM 915b)	ε^{40}Ca (SRM 915b)	$\delta^{44/40}$Ca (SRM 915a)*	ε^{40}Ca (SRM 915a)
Feb, session 1	0.56	0.07	0.04	4.22		
	0.49	0.04	0.02	4.14		
	0.40	0.01	-0.02	3.71		
	0.46	0.04	0.01	3.78		
	0.47	0.03	0.00	3.98		
	0.44	0.01	-0.04	4.18		
mean	0.47	0.03	0.00	4.00	0.66	3.54
2 s.e.				0.18		
Feb, session 2	0.42	0.00	-0.05	4.24		
	0.37	-0.04	-0.08	4.92		
	0.41	-0.02	-0.04	4.53		
	0.64	0.06	0.05	5.05		
	0.67	0.09	0.04	4.81		
	0.63	0.00	-0.02	6.20		
mean	0.52	0.01	-0.02	4.96	0.69	4.50
2 s.e.				0.55		
Mar. session 3	0.54	0.09	0.06	3.62		
	0.48	0.03	-0.05	4.17		
	0.52	0.05	-0.04	4.19		
	0.47	0.01	-0.01	4.49		
	0.45	0.00	0.05	4.39		
	0.50	0.04	-0.01	4.22		
	0.48	0.06	-0.02	3.49		
mean	0.49	0.04	0.00	4.08	0.64	3.62
2 s.e.				0.29		
Mar. session 3	0.64	0.07	-0.01	4.82		
	0.63	0.08	0.01	4.61		
	0.60	0.08	0.02	4.34		
	0.60	0.07	0.06	4.41		
	0.63	0.12	0.01	3.75		
	0.61	0.08	-0.03	4.43		
	0.65	0.11	0.03	4.23		
mean	0.62	0.09	0.01	4.37	0.54	3.91
2 s.e.				0.25		
Mar. session 3	0.48	0.05	0.05	3.71		
	0.52	0.07	0.11	3.80		
	0.51	0.04	0.01	4.19		
	0.56	0.09	0.00	3.81		
	0.51	0.06	-0.02	3.82		
	0.50	0.07	-0.01	3.59		
mean	0.51	0.06	0.03	3.82	0.59	3.36
2 s.e.				0.17		
Apr. session 4	0.52	0.01	0.00	4.91		
	0.48	0.03	0.07	4.14		
	0.49	0.02	-0.01	4.43		
	0.49	0.07	0.04	3.37		
	0.52	0.03	-0.07	4.37		
	0.56	0.06	-0.01	4.18		
	0.49	0.00	0.05	4.78		
mean	0.51	0.03	0.01	4.31	0.66	3.85
2 s.e.				0.38		

Table S-2 continued.

Analytical date	$\delta^{40/44}$Ca (SRM 915b)	$\delta^{42/44}$Ca (SRM 915b)	$\delta^{43/44}$Ca (SRM 915b)	ε^{40}Ca (SRM 915b)	$\delta^{44/40}$Ca (SRM 915a)*	ε^{40}Ca (SRM 915a)
Apr. session 4	0.48	0.06	0.11	3.68		
	0.52	0.08	0.03	3.61		
	0.55	0.06	0.06	4.18		
	0.53	0.05	0.08	4.22		
	0.54	0.05	0.07	4.37		
	0.55	0.07	-0.01	4.09		
	0.49	0.05	-0.03	3.76		
	0.54	0.06	0.01	4.24		
	0.53	0.03	-0.02	4.75		
	0.56	0.06	-0.04	4.44		
mean	0.53	0.06	0.03	4.13	0.60	3.67
2 s.e.				0.23		
Apr. session 4	0.51	0.06	0.02	3.87		
	0.53	0.06	0.03	4.26		
	0.50	0.00	0.02	4.93		
	0.51	0.04	0.03	4.03		
	0.55	0.06	-0.01	4.30		
	0.51	0.01	0.05	4.89		
	0.51	0.05	0.06	4.01		
	0.56	0.07	0.00	4.14		
	0.56	0.10	0.07	3.60		
	0.56	0.09	0.07	3.77		
	0.54	0.07	0.01	4.01		
mean	0.53	0.06	0.03	4.16	0.61	3.70
2 s.e.				0.25		
Total	0.53	0.05	0.01	4.22	0.62	3.76
2 s.e.				0.12		

*The value is calculated based on $\delta^{44/40}Ca_{SRM\ 915a} = 0.72 - \delta^{42/44}Ca \times 2.048$.

Table S-3 Ca isotope composition of planetary bodies and meteorites.

Table S-4 Melting of chondritic materials with evolving modal composition in melting residue.

Tables S-3 and S-4 (.xlsx) can be downloaded from the online version of this article at https://doi.org/10.7185/geochemlet.2302.

Supplementary Figures

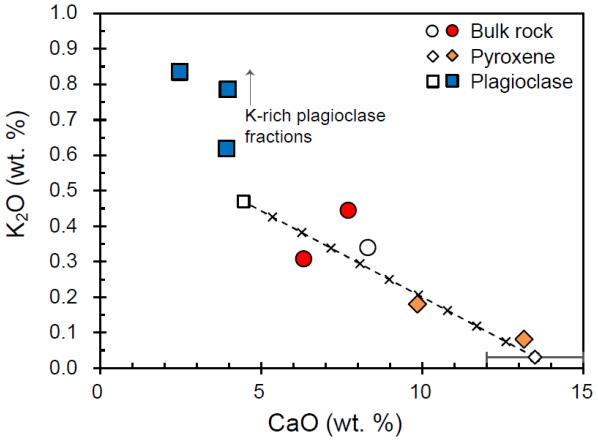

Figure S-1 K_2O *versus* CaO concentrations of separate minerals from EC 002 in this study. The composition of bulk rock, typical K-poor plagioclase and pyroxenes are shown for comparison (open dots) (Barrat *et al.*, 2021). The dashed line represents the mixing between typical pyroxenes and K-poor plagioclase and show good correlation with bulk rock fractions while the plagioclase fractions we selected show higher K_2O content.

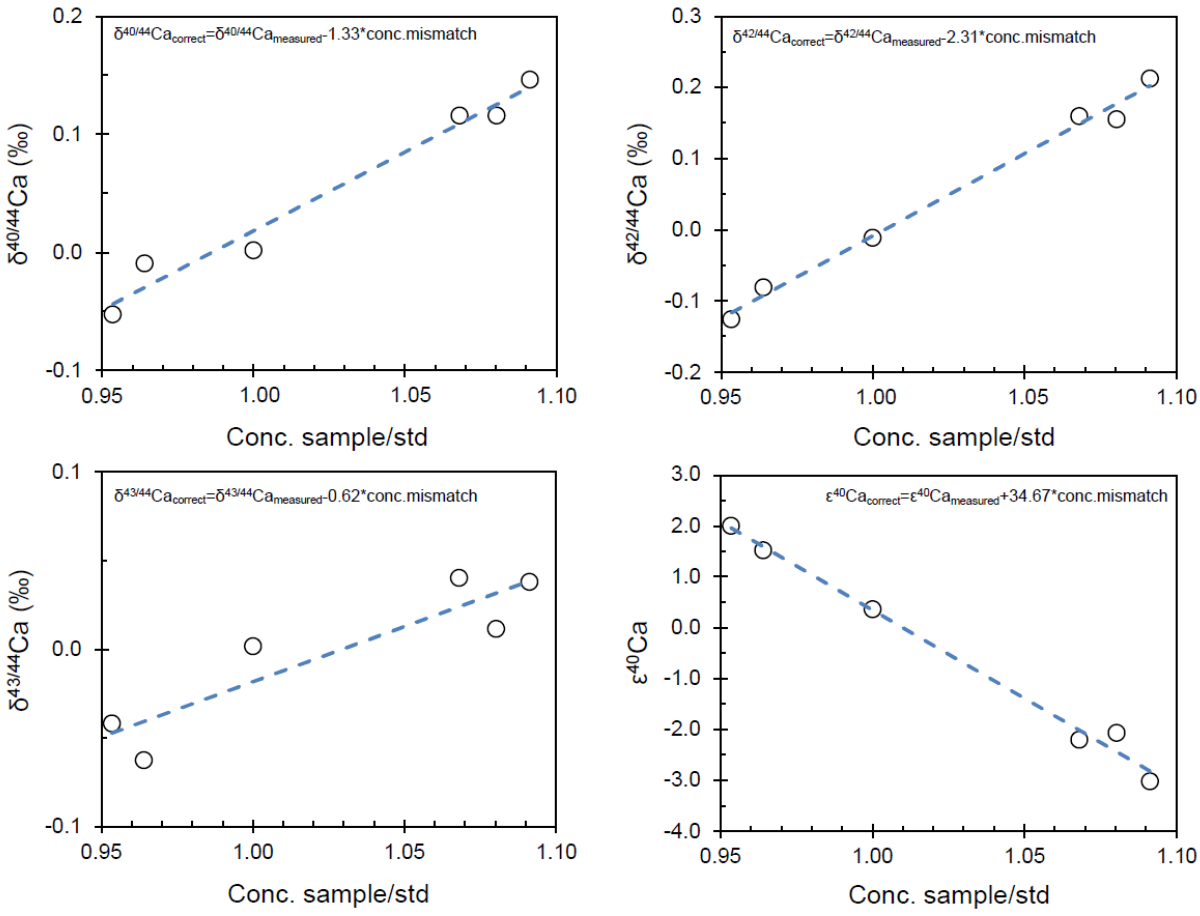

Figure S-2 Correction of concentration mismatch effects in session 2.

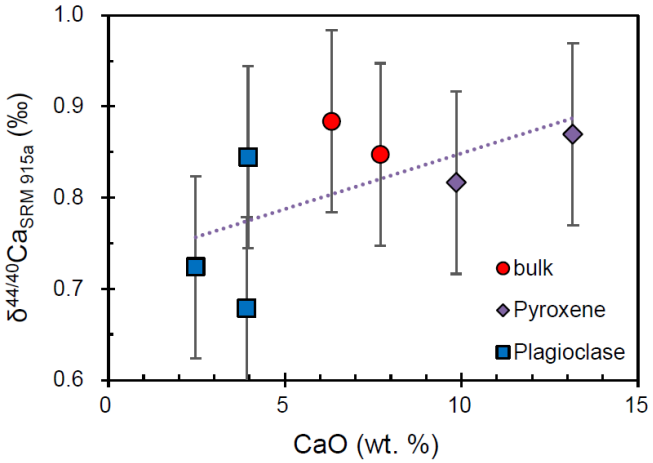

Figure S-3 $\delta^{44/40}$Ca *versus* CaO content of separates from EC 002 in this study. The pyroxenes show relatively higher $\delta^{44/40}$Ca values than plagioclases within error of bulk rock.

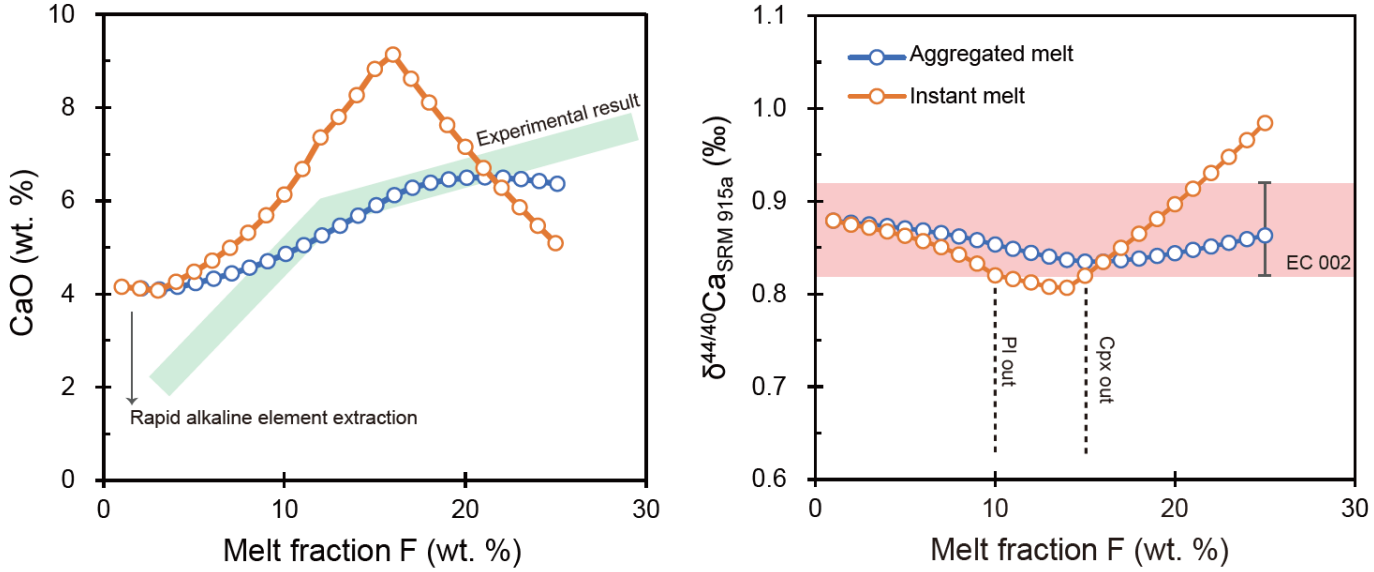

Figure S-4 Modelled **(a)** CaO content and **(b)** $\delta^{44/40}$Ca of melt with increasing degree of melting. The green area represents the melts from partial melting experiments of chondritic materials in literature (Collinet and Grove, 2020).

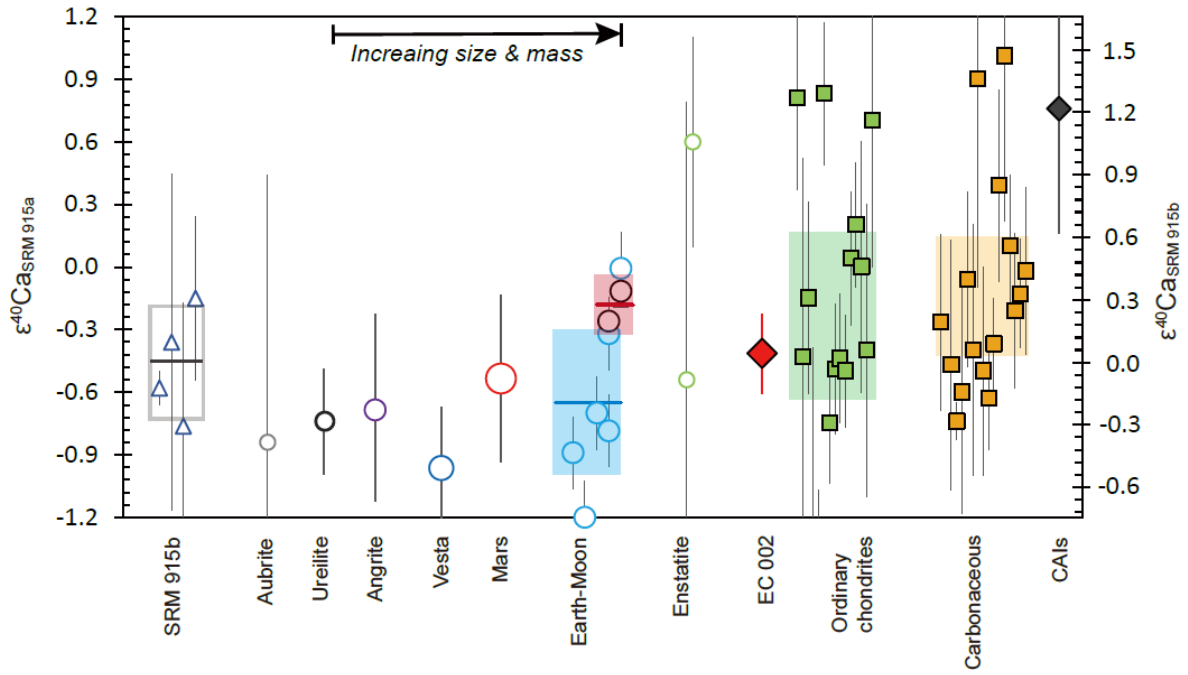

Figure S-5 Initial ε^{40}Ca values of different planetary bodies and meteorites. The ε^{40}Ca values of Angrite, Vesta and Mars are the average of relative samples from literatures (Simon *et al.*, 2009; Chen *et al.*, 2011; Huang and Jacobsen, 2017; Yokoyama *et al.*, 2017). Two ε^{40}Ca estimates of the bulk silicate earth are shown here: the blue square represents the average ε^{40}Ca of BSE obtained from terrestrial mafics and ultramafics (Simon *et al.*, 2009; Caro *et al.*, 2010; He *et al.*, 2017; Mills *et al.*, 2018; Antonelli *et al.*, 2019; Klaver *et al.*, 2021), and the red square represents ε^{40}Ca of the Earth-Moon system based on terrestrial and lunar samples (Caro *et al.*, 2010; Klaver *et al.*, 2021). The ε^{40}Ca of SRM 915b is also shown for comparison (Schiller *et al.*, 2012; Naumenko-Dèzes *et al.*, 2015; He *et al.*, 2017; Klaver *et al.*, 2021). The initial ε^{40}Ca value of EC 002 is consistent with the average ε^{40}Ca of ordinary chondrites (Simon *et al.*, 2009; Huang and Jacobsen, 2017; Yokoyama *et al.*, 2017).

Supplementary Information References

Amsellem, E., Moynier, F., Pringle, E.A., Bouvier, A., Chen, H., Day, J.M.D. (2017) Testing the chondrule-rich accretion model for planetary embryos using calcium isotopes. *Earth and Planetary Science Letters* 469, 75–83. https://doi.org/10.1016/j.epsl.2017.04.022

Antonelli, M.A., Simon, J.I. (2020) Calcium isotopes in high-temperature terrestrial processes. *Chemical Geology* 548, 119651. https://doi.org/10.1016/j.chemgeo.2020.119651

Antonelli, M.A., DePaolo, D.J., Chacko, T., Grew, E.S., Rubatto, D. (2019) Radiogenic Ca isotopes confirm post-formation K depletion of lower crust. *Geochemical Perspectives Letters* 9, 43–48. https://doi.org/10.7185/geochemlet.1904

Antonelli, M.A., DePaolo, D.J., Christensen, J.N., Wotzlaw, J.-F., Pester, N.J., Bachmann, O. (2021) Radiogenic ^{40}Ca in Seawater: Implications for Modern and Ancient Ca Cycles. *ACS Earth and Space Chemistry* 5, 2481–2492. https://doi.org/10.1021/acsearthspacechem.1c00179

Barrat, J.-A., Chaussidon, M., Yamaguchi, A., Beck, P., Villeneuve, J., Byrne, D.J., Broadley, M.W., Marty, B. (2021) A 4,565-My-old andesite from an extinct chondritic protoplanet. *Proceedings of the National Academy of Sciences* 118, e2026129118. https://doi.org/10.1073/pnas.2026129118

Bermingham, K.R., Gussone, N., Mezger, K., Krause, J. (2018) Origins of mass-dependent and mass-independent Ca isotope variations in meteoritic components and meteorites. *Geochimica et Cosmochimica Acta* 226, 206–223. https://doi.org/10.1016/j.gca.2018.01.034

Caro, G., Papanastassiou, D.A., Wasserburg, G.J. (2010) ^{40}K–^{40}Ca isotopic constraints on the oceanic calcium cycle. *Earth and Planetary Science Letters* 296, 124–132. https://doi.org/10.1016/j.epsl.2010.05.001

Chen, C., Dai, W., Wang, Z., Liu, Y., Li, M., Becker, H., Foley, S.F. (2019) Calcium isotope fractionation during magmatic processes in the upper mantle. *Geochimica et Cosmochimica Acta* 249, 121–137. https://doi.org/10.1016/j.gca.2019.01.031

Chen, H.-W., Lee, T., Lee, D.-C., Shen, J.J.-S., Chen, J.-C. (2011) ^{48}Ca Heterogeneity in Differentiated Meteorites. *The Astrophysical Journal Letters* 743, L23. https://doi.org/10.1088/2041-8205/743/1/l23

Collinet, M., Grove, T.L. (2020) Widespread production of silica- and alkali-rich melts at the onset of planetesimal melting. *Geochimica et Cosmochimica Acta* 277, 334–357. https://doi.org/10.1016/j.gca.2020.03.005

Dai, W., Moynier, F., Paquet, M., Moureau, J., Debret, B., Siebert, J., Gerard, Y., Zhao, Y. (2022) Calcium isotope measurements using a collision cell (CC)-MC-ICP-MS. *Chemical Geology* 590, 120688. https://doi.org/10.1016/j.chemgeo.2021.120688

Fang, L., Frossard, P., Boyet, M., Bouvier, A., Barrat, J.-A., Chaussidon, M., Moynier, F. (2022) Half-life and initial Solar System abundance of ^{146}Sm determined from the oldest andesitic meteorite. *Proceeds of the National Academy of Sciences* 119, e2120933119. https://doi.org/doi:10.1073/pnas.2120933119

Heuser, A., Eisenhauer, A. (2008) The Calcium Isotope Composition ($\delta^{44/40}$Ca) of NIST SRM 915b and NIST SRM 1486. *Geostandards and Geoanalytical Research* 32, 311–315. https://doi.org/10.1111/j.1751-908X.2008.00877.x

He, Y., Wang, Y., Zhu, C., Huang, S., Li, S. (2017) Mass-Independent and Mass-Dependent Ca Isotopic Compositions of Thirteen Geological Reference Materials Measured by Thermal Ionisation Mass Spectrometry. *Geostandards and Geoanalytical Research* 41, 283–302. https://doi.org/10.1111/ggr.12153

Huang, F., Zhou, C., Wang, W., Kang, J., Wu, Z. (2019) First-principles calculations of equilibrium Ca isotope fractionation: Implications for oldhamite formation and evolution of lunar magma ocean. *Earth and Planetary Science Letters* 510, 153–160. https://doi.org/10.1016/j.epsl.2018.12.034

Huang, S., Jacobsen, S.B. (2017) Calcium isotopic compositions of chondrites. *Geochimica et Cosmochimica Acta* 201, 364–376. https://doi.org/10.1016/j.gca.2016.09.039

Huang, S., Farkaš, J., Yu, G., Petaev, M.I., Jacobsen, S.B. (2012) Calcium isotopic ratios and rare earth element abundances in refractory inclusions from the Allende CV3 chondrite. *Geochimica et Cosmochimica Acta* 77, 252–265. https://doi.org/10.1016/j.gca.2011.11.002

Klaver, M., Luu, T.-H., Lewis, J., Jansen, M.N., Anand, M., Schwieters, J., Elliott, T. (2021) The Ca isotope composition of mare basalts as a probe into the heterogeneous lunar mantle. *Earth and Planetary Science Letters* 570, 117079. https://doi.org/10.1016/j.epsl.2021.117079

Lanping, F., Zhou, L., Yang, L., Zhang, W., Wang, Q., Shuoyun, T., Hu, Z. (2018) A rapid and simple single-stage

method for Ca separation from geological and biological samples for isotopic analysis by MC-ICP-MS. *Journal of Analytical Atomic Spectrometry* 33, 413–421. https://doi.org/10.1039/c7ja00370f

Li, M., Lei, Y., Feng, L., Wang, Z., Belshaw, N.S., Hu, Z., Liu, Y., Zhou, L., Chen, H., Chai, X. (2018) High-precision Ca isotopic measurement using a large geometry high resolution MC-ICP-MS with a dummy bucket. *Journal of Analytical Atomic Spectrometry* 33, 1707–1719. https://doi.org/10.1039/c8ja00234g

Liu, F., Zhu, H.L., Li, X., Wang, G.Q., Zhang, Z.F. (2017) Calcium Isotopic Fractionation and Compositions of Geochemical Reference Materials. *Geostandards and Geoanalytical Research* 41, 675–688. https://doi.org/10.1111/ggr.12172

Magna, T., Gussone, N., Mezger, K. (2015) The calcium isotope systematics of Mars. *Earth and Planetary Science Letters* 430, 86–94. https://doi.org/10.1016/j.epsl.2015.08.016

Mills, R.D., Simon, J.I., DePaolo, D.J. (2018) Calcium and neodymium radiogenic isotopes of igneous rocks: Tracing crustal contributions in felsic magmas related to super-eruptions and continental rifting. *Earth and Planetary Science Letters* 495, 242–250. https://doi.org/10.1016/j.epsl.2018.05.017

Moynier, F., Dai, W., Yokoyama, T., Hu, Y., Paquet, M., *et al*. (2022) The Solar System calcium isotopic composition inferred from Ryugu samples. *Geochemical Perspectives Letters* 24, 1–6. https://doi.org/10.7185/geochemlet.2238

Naumenko-Dèzes, M.O., Bouman, C., Nägler, T.F., Mezger, K., Villa, I.M. (2015) TIMS measurements of full range of natural Ca isotopes with internally consistent fractionation correction. *International Journal of Mass Spectrometry* 387, 60–68. https://doi.org/10.1016/j.ijms.2015.07.012

Russell, W.A., Papanastassiou, D.A., Tombrello, T.A. (1978) Ca isotope fractionation on the Earth and other solar system materials. *Geochimica et Cosmochimica Acta* 42, 1075–1090. https://doi.org/10.1016/0016-7037(78)90105-9

Schiller, M., Paton, C., Bizzarro, M. (2012) Calcium isotope measurement by combined HR-MC-ICPMS and TIMS. *Journal of Analytical Atomic Spectrometry* 27, 38–49. https://doi.org/10.1039/c1ja10272a

Schiller, M., Bizzarro, M., Fernandes, V.A. (2018) Isotopic evolution of the protoplanetary disk and the building blocks of Earth and the Moon. *Nature* 555, 507–510. https://doi.org/10.1038/nature25990

Simon, J.I., DePaolo, D.J. (2010) Stable calcium isotopic composition of meteorites and rocky planets. *Earth and Planetary Science Letters* 289, 457–466. https://doi.org/10.1016/j.epsl.2009.11.035

Simon, J.I., DePaolo, D.J., Moynier, F. (2009) Calcium Isotope Composition of Meteorites, Earth, and Mars. *The Astrophysical Journal* 702, 707–715. https://doi.org/10.1088/0004-637x/702/1/707

Stöffler, D., Hamann, C., Metzler, K. (2018) Shock metamorphism of planetary silicate rocks and sediments: Proposal for an updated classification system. *Meteoritics & Planetary Science* 53, 5–49. https://doi.org/10.1111/maps.12912

Valdes, M.C., Moreira, M., Foriel, J., Moynier, F. (2014) The nature of Earth's building blocks as revealed by calcium isotopes. *Earth and Planetary Science Letters* 394, 135–145. https://doi.org/10.1016/j.epsl.2014.02.052

Valdes, M.C., Bermingham, K.R., Huang, S., Simon, J.I. (2021) Calcium isotope cosmochemistry. *Chemical Geology* 581, 120396. https://doi.org/10.1016/j.chemgeo.2021.120396

Wang, W., Zhou, C., Qin, T., Kang, J.-T., Huang, S., Wu, Z., Huang, F. (2017) Effect of Ca content on equilibrium Ca isotope fractionation between orthopyroxene and clinopyroxene. *Geochimica et Cosmochimica Acta* 219, 44–56. https://doi.org/10.1016/j.gca.2017.09.022

Wang, Y., He, Y., Wu, H., Zhu, C., Huang, S., Huang, J. (2019) Calcium isotope fractionation during crustal melting and magma differentiation: Granitoid and mineral-pair perspectives. *Geochimica et Cosmochimica Acta* 259, 37–52. https://doi.org/10.1016/j.gca.2019.05.030

Williams, H.M., Bizimis, M. (2014) Iron isotope tracing of mantle heterogeneity within the source regions of oceanic basalts. *Earth and Planetary Science Letters* 404, 396–407. https://doi.org/10.1016/j.epsl.2014.07.033

Yokoyama, T., Misawa, K., Okano, O., Shih, C.-Y., Nyquist, L.E., Simon, J.I., Tappa, M.J., Yoneda, S. (2017) Extreme early solar system chemical fractionation recorded by alkali-rich clasts contained in ordinary chondrite breccias. *Earth and Planetary Science Letters* 458, 233–240. https://doi.org/10.1016/j.epsl.2016.10.037

Zhang, H., Wang, Y., He, Y., Teng, F.-Z., Jacobsen, S.B., Helz, R.T., Marsh, B.D., Huang, S. (2018) No Measurable Calcium Isotopic Fractionation During Crystallization of Kilauea Iki Lava Lake. *Geochemistry, Geophysics, Geosystems* 19, 3128–3139. https://doi.org/10.1029/2018gc007506